ELSEVIER

Nuclear Instruments and Methods in Physics Research B 150 (1999) 173–178

NIM B
Beam Interactions with Materials & Atoms

3D mapping of individual cells using a proton microbeam

C. Michelet, Ph. Moretto *

Centre d'Etudes Nucléaires de Bordeaux Gradignan, BP 120, 33175 Gradignan, France

Abstract

Various imaging techniques carried out with a nuclear microprobe make it possible to reveal by 2D mapping, the internal structure of isolated cells. An improvement of those techniques allows today 3D mapping of cells. STIM- and PIXE-Tomography have been recently implemented on the CENBG microbeam line. The performance offered by these methods, which are capable of resolving objects having diameters less then 100 μm, has been validated on reference specimens and on human cells from cultures. In addition to the fineness of the resolution, these techniques offer the advantage of performing volume analyses without prior cutting of the samples. The ultimate aim of this program of research is to perform 3D elemental chemical analysis of individual cells in the field of biomedicine. © 1999 Elsevier Science B.V. All rights reserved.

PACS: 87.64.-t; 87.59.Fm; 87.22.Bt; 29.30.Kv
Keywords: Subcellular structure; Computed tomography; X-ray analysis; Cultured cells; Ion microbeam; Microscopy

1. Introduction

The first applications of real 3D mapping using STIM-Tomography (STIM-T) appeared at the end of the eighties [1]. The principle of PIXE-Tomography (PIXE-T) in its ultimate form was only reported a few years later by Schofield and Lefevre [2]. This analysis of a scorpion stinger constituted one of the first examples of 2D tomography in the life sciences. Although this technique is well suited to the analysis of biological specimens, very few studies have been published since then in this field. The range of MeV ions, more especially protons, in organic material is sufficient to probe large biological structures, cell aggregates or even individual cells. Thus it is possible to map the inner structure of the object under investigation without sectioning it.

STIM-T and PIXE-T techniques have been recently developed in Bordeaux using the CENBG microbeam line. Our group benefits of a long experience in the 2D analysis of cultured cell lines [3], more particularly at the cellular and subcellular level. The present study was conducted in the framework of this program. The aim was to demonstrate, for the first time, the capability of ion micro-tomography to elucidate the ultrastructure of a mammalian cell. Our experimental setup will be first briefly presented as also the analytical procedure. Then, results of STIM-T and

* Corresponding author. Tel.: +33-5-57120896; fax: +33-5-57120801; e-mail: moretto@cenbg.in2p3.fr

0168-583X/99/$ – see front matter © 1999 Elsevier Science B.V. All rights reserved.
PII: S0168-583X(98)01015-5

PIXE-T analyses of individual cells will be compared and some methodological points evoked.

2. Material and methods

2.1. Cell line and sample preparation

Cells aimed for tomography analysis were prepared as follows: A human ovarian adenocarcinoma cell line, IGROV1 [4], was cultured on thin Formvar films under experimental conditions reported earlier [5]. The cell monolayer obtained was then cryofixed in isopentane chilled with liquid nitrogen and freeze-dried for several hours at −30°C. Individual cells selected under light microscopy for their morphological characteristics and preservation status were picked up using thin micro-pipettes and fixed on the tip of a glass micro-capillary (30 μm in diameter) using high polymerizing speed Araldite™ glue. The capillary was then inserted in a larger tube easier to manipulate.

In order to validate the performance of the technique, we prepared also reference specimens with a simple structure consisting of microscopic (4–7 μm) nickel grains (Goodfellow™) embedded in a Formvar polymer matrix. A regular cylindrical wire (80 μm in diameter) was obtained and fixed at the extremity of a larger glass capillary.

2.2. Experimental setup

The 3D analyses have been performed using the CENBG microbeam line, an experimental setup previously described [6]. In the STIM configuration, the angular divergence of the beam penetrating the optics was limited using two 5-μm circular apertures, one defining the object and the second placed at a distance of 5.4 m, in front of the first quadrupole. In this way, the beam intensity on the target was reduced down to about 1500 protons/s with a spatial resolution below 1 μm. For 3D PIXE analysis, the object diameter was increased up to 20 μm and the second collimator to 1 mm in order to achieve a beam intensity of 200 pA with a 2-μm spot on the sample. STIM and PIXE analyses were both performed with 3.0-MeV protons for the reference specimen and 2.8-MeV protons for individual cells.

In the irradiation chamber, samples were mounted, using a small-dimension mandrel, fixed directly on the rotating axis of a high-precision computer-controlled step motor. To avoid any problem of temperature rise under vacuum and thus dilatation effect, the motor was mechanically coupled to a water-cooled copper mass by means of a high thermal conducting braid. For STIM analysis, a 200-mm^2 ion-implanted-silicon charged-particle detector was placed on beam axis 1 cm behind the sample on a retractable holder. For PIXE analysis, a 60-mm^2 Si(Li) X-ray detector was placed at 135° at a distance of 2 cm from the specimen axis.

2.3. Analytical procedure

Since the specimen damage caused by STIM is quite negligible, STIM-T was carried out prior to PIXE-T. Moreover, the time required for the PIXE analysis of a single slice is so prohibitive (about 1 h) that only a few horizontal sections were investigated. Anyway, the complete 3D structure provided by STIM gave meaningful information for the interpretation of the PIXE tomographic slices.

For 3D STIM-T analysis, the following procedure has been employed: 100 angular projections were performed rotating the sample over 180° with a step of 1.8°. For each projection, a 2D vertical (128×64 points) scan was carried out measuring the residual energy of the transmitted ions. The 64 horizontal tomographic slices composed of 128×128 voxels were then numerically reconstructed, each separately, in order to provide a complete 3D map of the specimen density. The duration of this analysis was typically 2.5 h and the total reconstruction achieved within 30 min on a SUN UltraSparc workstation. The cell, presented in Fig. 2, was mapped with a 2D scan size of 166×166 μm^2. The spatial resolution was limited here by a voxel size of about $1.3 \times 1.3 \times 2.6$ μm^3. Individual slices of the same cell were then

submitted to PIXE-T analysis. In this case, the same number of projections were employed, but each projection simply consisted of a linear scan (128 points).

A horizontal slice of the reference specimen was also mapped using both PIXE-T and STIM-T. For each angular projection, a linear scan was carried out over 109 μm. For STIM-T, the particle detector was moved every 20 projections to prevent any damage due to the high beam fluence.

2.4. 3D reconstruction

STIM-T is based on the assumption that the slowing down of the particle crossing the sample is directly related to the areal density of the material. In the present study, the residual energy of particles was measured at a specific beam position using the median value. The energy loss was then converted into an areal density using a method initially proposed by Lefevre and Schofield [7]. In this calculation, modified routines of the source code RUMP [8] were used to compute the stopping power on the basis of a least squares fit (from 350 to 3500 keV) of tabulated values by Andersen and Ziegler [9]. For compound materials, the stopping powers were calculated using Bragg's rule. As previously shown [7], this calculation was found to be rather unsensitive to the specimen composition, especially for biological specimens. For the reconstruction of the individual cell, we assumed a $C_{10}H_8O_{0.8}N_{1.3}$ composition, previously derived from the Rutherford Back-Scattering analysis of cells from the IGROV1 line.

Since the beginning of Computed Tomography, about 30 years ago, various reconstruction algorithms have been developed. For low-noise data such as STIM-T data, the best suited is filtered back-projection. In this work, we used routines of Donner library [10], initially developed for X-ray tomography. 3D reconstruction of PIXE data is more complex in the sense that the decrease in X-ray yields with the slowing down of the incident ion, as also the auto-attenuation of X-rays, must be taken into consideration. To solve this problem, reconstruction algorithms based on iterative methods have been proposed by Schofield and Lefevre [2], and Antolak and Bench [11]. In these methods, the 3D density map of the object, determined in a first step by STIM-T, allows the computing of an effective attenuation factor to correct the PIXE-T reconstruction. Since we have not developed such a complete data treatment yet, we used filtered back-projection to treat PIXE data. The PIXE-T reconstruction was performed using a smoothing Hann filter. The effect of this filter is conspicuous comparing the STIM maps (a) and (b) in Fig. 3, reconstructed, respectively, with a ramp and Hann filter.

2.5. Rotation center

An important point concerning the data reduction was to define the position of the experimental rotation center. A good precision was required, since even a single pixel error on its location would have led to important recon-

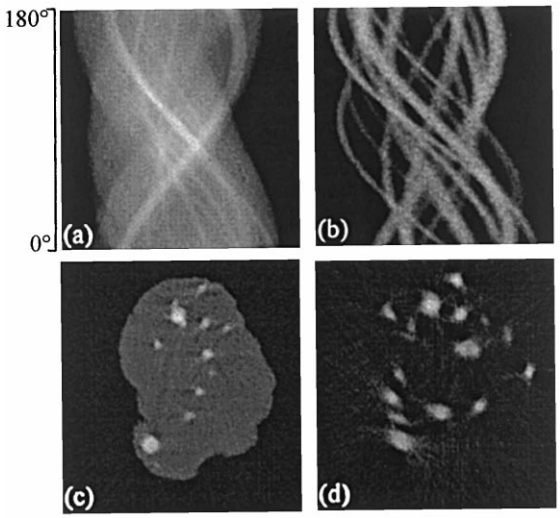

Fig. 1. 2D STIM and PIXE tomography of a reference specimen slice: (a) STIM sinogram, coded on a 25 levels gray scale spanning from zero (black) to 13.8 g/cm^2 (white). This sinogram consists of 100 horizontal lines (128 points over 109 μm), one per angular projection. (b) PIXE sinogram of the nickel distribution constructed using the K_α line yield, ranging from zero (black) to maximum (white, 548 events per point). The sinusoidal pattern on both sinograms is due to nickel containing grains. (c) STIM-T and (d) PIXE-T reconstructions (128 × 128 voxels) using a ramp filter. Nickel grains down to ~3 μm wide are visible on both images.

struction artifacts. For STIM-T, we determined the rotation center using a least squares algorithm according to Azevedo et al. [12]. This procedure makes use of the sinusoidal patterns described by all points of the sinogram (Fig. 1). The position of the center of mass on the sinogram is computed at each projection. These positions are then fitted to a sinusoidal function whose symmetry axis defines the rotation center. For PIXE-T, however, no reference point is available in the projection data. A test reconstruction is performed with the same rotation center as for STIM-T, then its position is adjusted until typical asymmetric artefacts (known as "tuning-fork artefacts") are minimized.

3. Results and discussion

The reference specimen STIM-T and PIXE-T analyses are compared in Fig. 1. Nickel grains of size down to 3 μm can be distinguished on both the reconstructed 2D maps, displaying, respectively, the density and the nickel distributions in the same slice. What is striking is that more nickel grains are revealed by PIXE-T. This can be partly explained by the difference in spatial resolution offered by the two techniques. The beam size is larger for PIXE-T, and so is consequently the thickness of the probed specimen slice. Moreover an uncertainty of a few microns on the beam position when turning the beam line from STIM to PIXE configuration

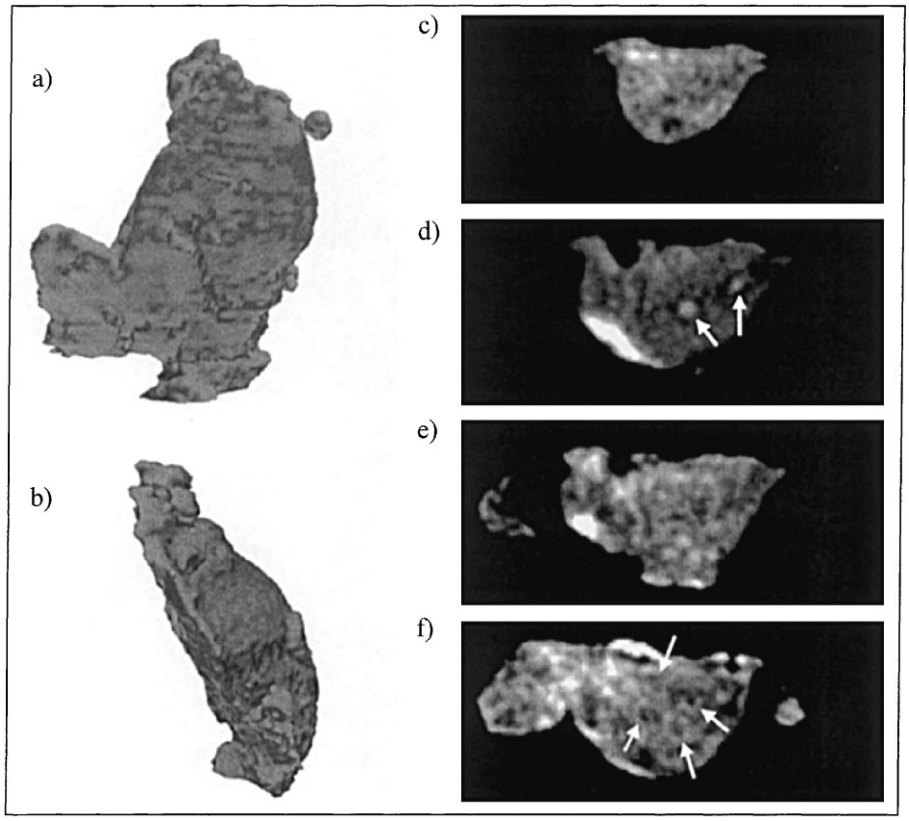

Fig. 2. 3D STIM tomography of an individual cell: front view (a) and side view (b) of the external envelop. Smaller cells attached on the top and the side are also visible. The dimension of the scan was 166×166 μm^2 and a total of 64 horizontal slices were analyzed. Maps (c)–(f) (166×70 μm^2) represent, respectively, the slices number 24, 33, 37 and 44, from the top to the specimen bottom. A Hann filter (cut-off frequency 0.5) was used in the reconstruction to smooth the data. Maps (c), (d) and (f) have been plotted using a 25 gray levels scale ranging from 0.054 (black) to 0.154 g/cm^3 (white) whereas the (e) scale ranges from 0.069 to 0.231 g/cm^3. The arrows indicate nuclear lobes on slice (f) and high density nucleoli on slice (d).

may be put forward. These two reasons could lead to the exploration of specimen plans at slightly different heights. Regarding the reconstruction process of STIM data, one has to stress here that the assumption of fairly homogeneous composition is not verified. Concerning PIXE data, the correction of X-ray yields and attenuation must be also taken into account in this kind of specimen. It is obvious that the reduction of these tomographic data requires a more complex iterative algorithm that we have not yet implemented.

A complete 3D STIM analysis of an individual human ovarian cell is presented in Fig. 2. Two views of the cell's external structure at different angles have been plotted using a software developed at CENBG in the PHIGURE™ library graphic environment. The external envelope of the specimen has been constructed selecting the isosurface at the zero density threshold. The cell line used in this study usually grows under different morphotypes: small mononucleated cells, about 15 μm in diameter, and much larger polynucleated cells, more than 50 μm wide [5]. The cell presented in the figure is a specimen from the second population. A few small round cells having grown in its vicinity remained nevertheless attached during the sampling procedure and can be easily recognized on the cell surface. In Fig. 2(b), the flat shape of the basal face, that was attached to the culture support, has been preserved.

Four horizontal slices, chosen at different heights, have been plotted in the same figure. The interpretation of such a new kind of image is not straightforward due to the fact that the specimen was dehydrated. The density gradient of the organic material does not delimit necessarily the different cell organelles. Nevertheless, some typical features of the cellular ultrastructure are clearly visible; especially, several round nuclear lobes, one of the main characteristics of this polynucleated cell line, appear on slice (f). In addition, nucleoli may be identified by bright points on the slice (d). This observation is consistent with the 2D STIM analysis we performed previously on this cell line [3]. The nucleoli had been identified as the organelles with the highest density within cells.

In Fig. 3, STIM-T and PIXE-T analyses of a particular slice of the same cell are compared.

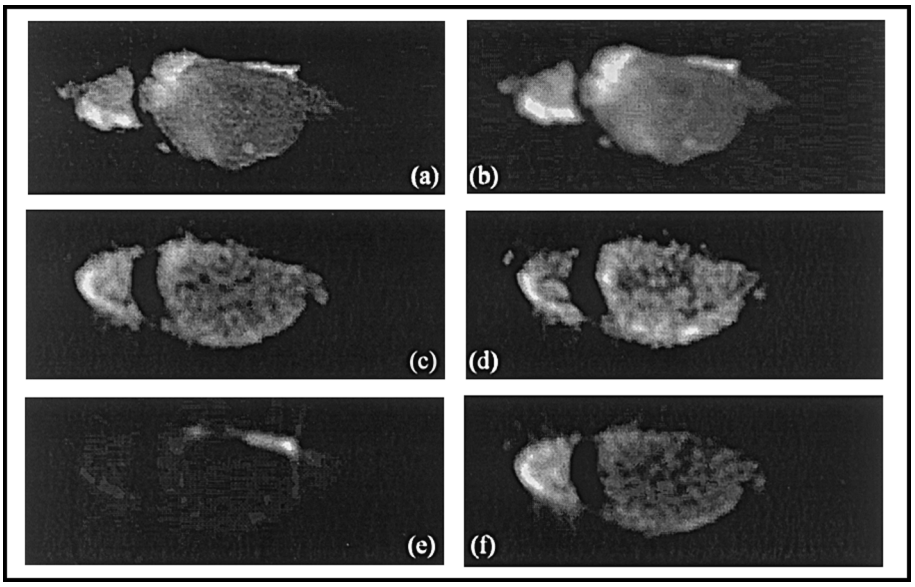

Fig. 3. Comparison of 2D STIM-T and PIXE-T analyses of the slice number 51 (same cell as in Fig. 2). These maps have been reduced from 128×128 voxels to 128×54 voxels (i.e.166×70 μm^2) for clarity. STIM-T maps reconstructed using a filtered back-projection algorithm with (a) ramp filter, (b) Hann filter (cut-off frequency 0.5). (c)–(f) PIXE-T maps of potassium, phosphor, sulfur and chlorine, respectively.

Potassium, phosphorus, sulfur and chlorine maps have been reconstructed using the respective K lines. A slight distortion appears in the cell shape presumably due to the restriction evoked earlier on the analyzed plan. The high density structure which appears on the top right of (a) and (b) was found to be characterized by a high sulfur level, as demonstrated on the sulfur map (e). This contamination is certainly due to the sulfur-containing glue employed to fix the cell on the micro-capillary.

4. Concluding remarks

This study demonstrated the capability of ion micro-tomography to determine the subcellular ultrastructure using the 3D density map. It is obvious that a great deal of work in collaboration with biologists is still necessary to interpret unambiguously such pictures. Moreover, these studies will have to be carried out using cell lines with a more simple structure than the polynucleated cells employed here. Great efforts will be also necessary to adapt the culture and specimen-mounting techniques in order to avoid absolutely the use of glue and the consequent possible contamination. Among the main advantages of this technique in biological applications are: (i) the inner structure can be elucidated without any sectioning procedure; (ii) the analysis can be performed on a virgin cell, just cryofixed and freeze-dried.

Acknowledgements

The authors wish to acknowledge Dr. R. Ortega for his help in providing the cultured cells.

References

[1] A.E. Pontau, A.J. Antolak, D.H. Morse, A.A. Berkmoes, J.M. Brase, D.W. Heikkinen, H.E. Martz, I.D. Proctor, Nucl. Instr. and Meth. B 40 (1989) 646.
[2] R.M.S. Schofield, H.W. Lefevre, Nucl. Instr. and Meth. B 72 (1992) 104.
[3] P. Moretto, Y. Llabador, R. Ortega, M. Simonoff, L. Razafindrabe, Nucl. Instr. and Meth. B 75 (1993) 511.
[4] J.R. Teyssier, J. Bénard, D. Ferre, J. Da Silva, L. Renaud, Cancer Genet. Cytogenet. 39 (1989) 35.
[5] R. Ortega, Ph. Moretto, A. Fajac, J. Bénard, Y. Llabador, M. Simonoff, Cell. Mol. Biol. 42 (1) (1996) 77.
[6] Y. Llabador, Ph. Moretto, Applications of Nuclear Microprobes in the Life Sciences, World Scientific, Singapore, 1998.
[7] H.W. Lefevre, R.M.S. Schofield, Scanning Microsc. 1 (1987) 879.
[8] L.R. Doolittle, Nucl. Instr. and Meth. B 9 (1985) 344.
[9] H.H. Andersen, J.F. Ziegler, Hydrogen Stopping Powers and Ranges in All Elements, Pergamon Press, New York, 1977.
[10] R.H. Huesman, G.T. Gullberg, W.L. Greenberg, T.F Budinger, RECLBL Library Users Manual, Pub. 214, Lawrence Berkeley Laboratory, 1977.
[11] A.J. Antolak, G.S. Bench, Nucl. Instr. and Meth. B 88 (1994) 297.
[12] S.G. Azevedo, D.J. Schneberk, J.P. Fitch, H.E. Martz, IEEE Trans. Nucl. Sci. 37 (4) (1990) 1525.